Draft version May 16, 2021
Typeset using LaTeX default style in AASTeX63

Dust In The Wind: The Search for Dust In the Outflows of Low Mass Protostar HH212

Hannah Shoemaker[1]

[1] *University of Virginia, Departments of Astronomy and Physics*

ABSTRACT

Star formation is a chemically and physically complex process that begins in dense molecular clouds and ends in the formation of planets. During the star formation process some young protostars have been observed with molecular outflows, which are collimated jets of molecular gas. The launching mechanism for these outflows is still unknown, but there are many theories that attempt to describe the launching region in relation to stellar, disk and x-winds. The presence of dust inside protostellar disk winds has been suggested but never observationally confirmed. The observational detection of dust in the region of protostellar disk winds would put constraints upon the dust content of outflows as well as the initial conditions for planet formation around low mass protostars. I am investigating the dust content in the winds emanating from young (Class 0 and Class I) systems. This study began with an archival search using the ALMA Science Archive, resulting in a list of low mass protostellar sources observed with sufficiently high angular resolution. Next, preliminary inspection of the images was done by an affiliated student group to determine the best candidates for the detection of dust. I performed extensive re-imaging of multi-band observations from HH212 to constrain the dust content in outflows. Ongoing work will analyze the characteristics of the dust content, comparing models with observations to explain the mechanism for dust entrainment in protostellar winds.

1. INTRODUCTION

The star formation process (Figure 1) begins in dense regions of gas and dust called molecular clouds. When a gravitational collapse occurs the cloud becomes smaller and the rotational speed increases. Eventually the material in the cloud forms a disk around the protostellar core with a Keplerian rotation profile. To conserve angular momentum the protostar is ejecting material in bipolar jets perpendicular to the rotating accretion disk, which is possibly pre-planetary in nature. These highly collimated bipolar jets of atomic and molecular gas are also called outflows. The combination of strong magnetic fields, rotation and gravity in protostellar jets causes the ejection of material from the surface of the accretion disk and into the envelope. This material is primarily molecular gas and outflows can be detected using characteristic emission lines of molecules that make up the gas being accelerated. Outflows are prominent in the Class 0 and Class 1 stages of star formation, and become less distinguishable in the later stages of stellar evolution. The protostellar core eventually reaches temperatures high enough to achieve fusion and it is believed that the circumstellar disk will go on to form planetary systems. The first step of planet formation is the coagulation of dust grains into incrementally larger aggregates until a planetesimal is formed. The dust grains grow from sub-micron sized grains, found in the early stages of star formation, to the larger bodies that form in the dense mid-plane of protoplanetary disks (Testi et al. 2014). ALMA, The Atacama Large Millimeter/Sub-millimeter Array, is an interferometer in Chile optimized for studying the cold universe, including gas and dust around young stars. ALMA has been instrumental in establishing observational constraints on the models of planetary evolution.

The exact launching mechanism of the outflow is still unknown, but there are three primary theories that differ mainly in the identification of the launching region of the outflow. The first theory is that of a stellar wind which is thought to emanate from the poles of the protostar (Bouvier et al. 2014). The second theory is that of a so-called 'x-wind', which is the phenomena that results from magnetic field interaction between the protostellar fields and the disk fields (Shang et al. 2006). The third, and currently the most popular theory, is that of the disk wind: a magnetically ejected 'wind' emanating across an extended region of the accretion disk (Frank et al. 2014). It is likely that the true launching mechanism is a combination of these theories. A schematic showing the locations of the disk wind and x-wind is shown in Figure 2.

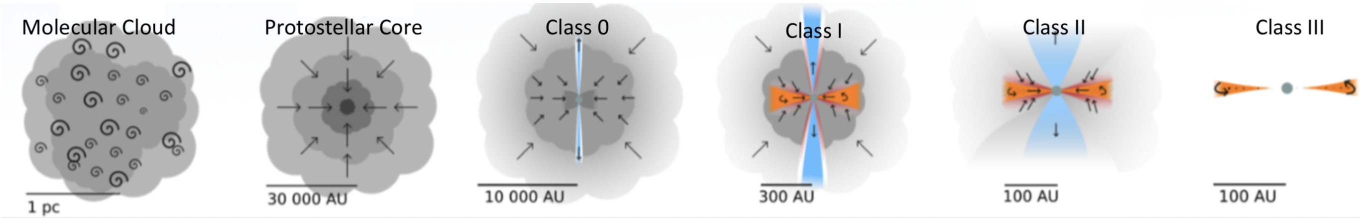

Figure 1: A figure illustrating the star formation process. Star formation begins in molecular clouds which undergo a collapse. A rotating protostellar disk is left surrounding the protostar. Jets of collimated gas are ejected, forming the outflow. Disk accretion continues until the outflow slows down and the process of planetary formation through pebble accretion begins. Blue regions of the diagram indicate a molecular outflow and orange indicate an accretion disk (Persson 2014).

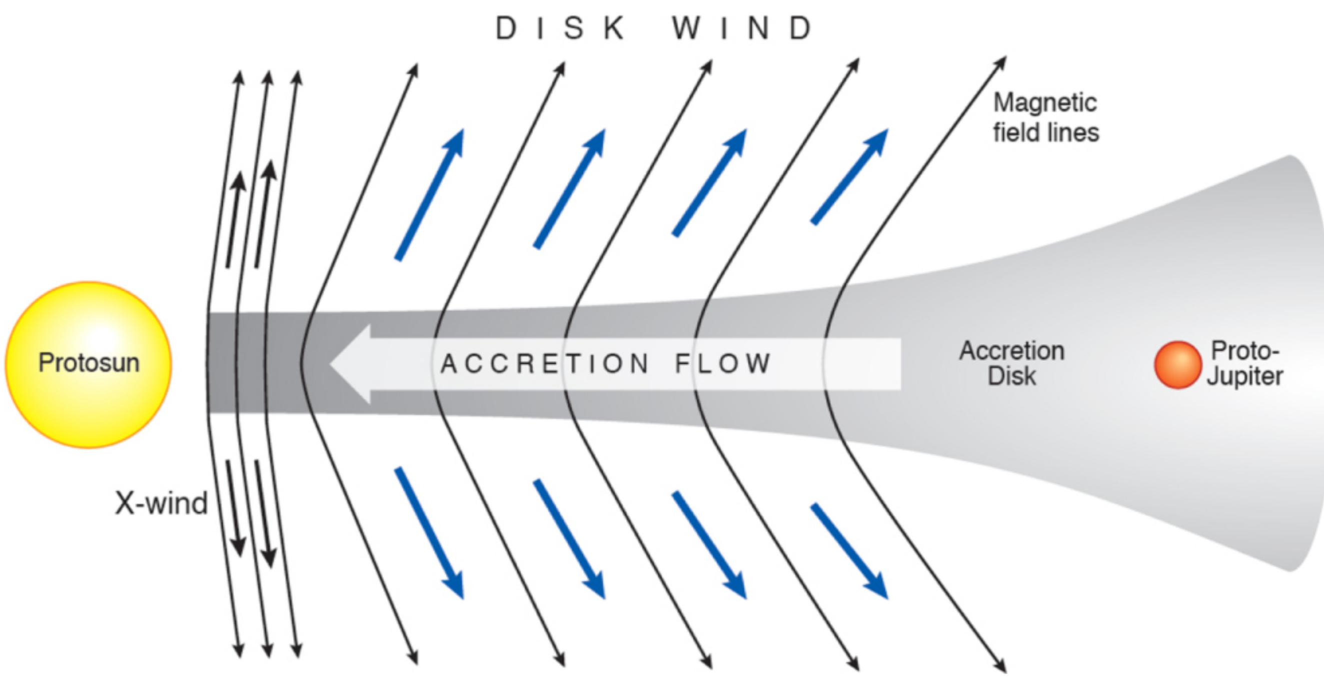

Figure 2: The figure illustrates the relationship between the disk wind, the accretion disk and the x-wind.(Figure 4. from Isotopic Dichotomy among meteorites and Its Bearing on the Protoplanetary Disk.) Scott et al. (2018)

.

If the disk wind is responsible for accelerating the molecular gas from the accretion disk into the surrounding envelope, we expect that it also sweeping up and launching sub-millimeter dust particles. A detection of dust may constrain the launch region of the jet, and give an indication as to the launch mechanism. Furthermore, if significant quantities of dust are being lifted from the disk, it is cause to reevaluate the theory on disk evolution. The amount of dust present in the accretion disk has significant implications for the initial conditions of planet formation in young protostellar systems.

To begin this study we conducted a thorough archival search of the ALMA Science Archive (ASA). We programmatically searched the archive by querying the ASA for sources that met certain criteria: the source must have an outflow, and observations must have been made with a higher resolution than 0.2” (less than ~100 AU at the distance of many protostars). We retained sources that had a known outflow, were not perfectly face on (as this would make any dust in the outflow indistinguishable from the dust in the accretion disk), and had multi-band observations. The resulting list of protostars included only young (Class 0 and Class I), non-binary, low-mass stars. Three sources: HH212, B228 (IRAS15398-3359), and B335 were selected as being the most interesting for further investigation. Preliminary investigations suggested that there was extension in each of these sources and the extension in B228 and B335 can be seen in Figure 3. Tabone et al. (2020),Lee et al. (2018) shows the existence of a disk wind in HH212, although there is not yet resolved data of the launching region for B335 or B228. This paper presents data from ALMA Cycles 1, 3, 4 and 5 to more closely examine the extension in the continuum of HH212 in the region of the wind.

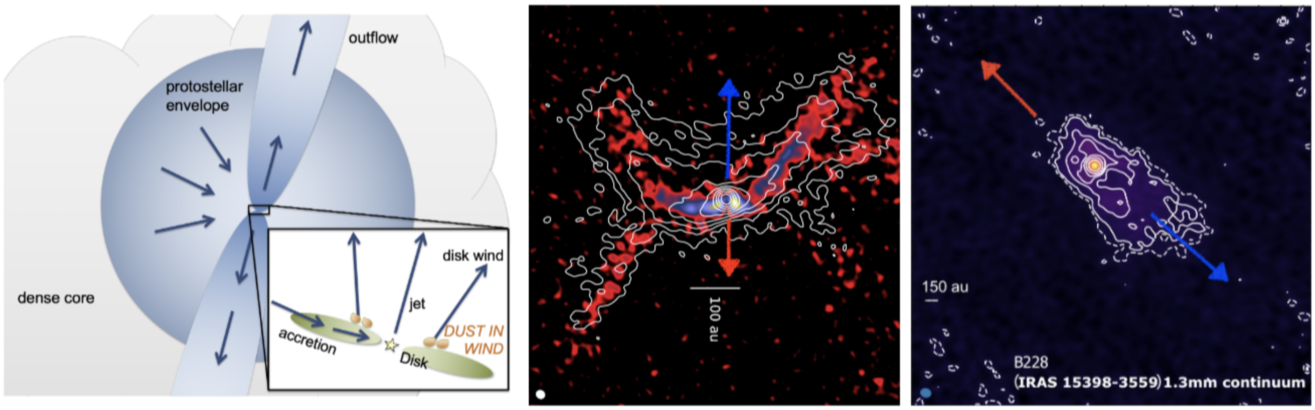

Figure 3: The aim of this project was to search the ALMA Science Archive for existing data which show regions of protostellar objects where dust may be present in the disk wind (orange text in left panel)(Bjerkeli, private communication). (center, Yen et al. (2020)) An example of B335 where dust continuum emission traces the shape of the known molecular outflow. (right) Continuum emission in IRAS 15398 (B228) re-imaged from 2013.1.00879.S. Blue and red arrows indicate the axis of the respective outflows. Continuum extensions have been previously noted in the literature, but there has been no observational confirmation of the phenomenon we call dust in the wind.

HH212 is a Class 0 protostellar system located at ∼400pc in the L1630 cloud of Orion (Kounkel et al. 2018). It is one of the first and best vertically resolved disks, and is nearly edge on with an inclination angle of -4°(reference). HH212 has a well studied symmetrical, bipolar outflow with an axis of -23° (Claussen et al. 1998). The central protostar of the HH212 system is estimated to have a mass of $0.25 \pm 0.05\ M_{\odot}$ from Lee et al. (2017), and this mass is confirmed with our own calculations. HH212 is a well studied object and the multitude of multi-band observations available for public use in the ASA makes it a unique target for a variety of scientific goals.

2. OBSERVATIONAL RESULTS

The ALMA Science Archive contains data for HH212 in ALMA Bands 3(115.27 GHz), 6(230.5 GHz), 7(345.7 GHz) and 9(691.47 GHz). Figure 5 shows an image for each of these bands, all of which we re-imaged to get better sensitivity. In addition to the natural parameters the images are presented at convolved beam and cell sizes so that more direct comparisons can be made. Special attention was given to the Band 7 data because the most data were availabe for this band. Working with data analysts at the National Radio Astronomy Observatory, a high resolution 345 GHz continuum image was produced by combining data from four projects: 2012.1.00122.S, 2015.1.00024.S, 2016.1.01475.S and 2017.1.00044. There were a total of 76 spectral windows with continuum emission across these projects. Each spectral window was individually examined and any channels displaying strong line emission were removed. The projects were combined using the tclean task of the Common Astronomy Software Application (CASA) package version 5.6.1 with Briggs weighting (robust =0.5, which balances between sensitivity and angular resolution), in order to obtain an image with more sensitivity than was previously available. The results of this combination are presented in Figure 4. Further information about the observational parameters for each individual project can be found in Table 3 in the appendix.

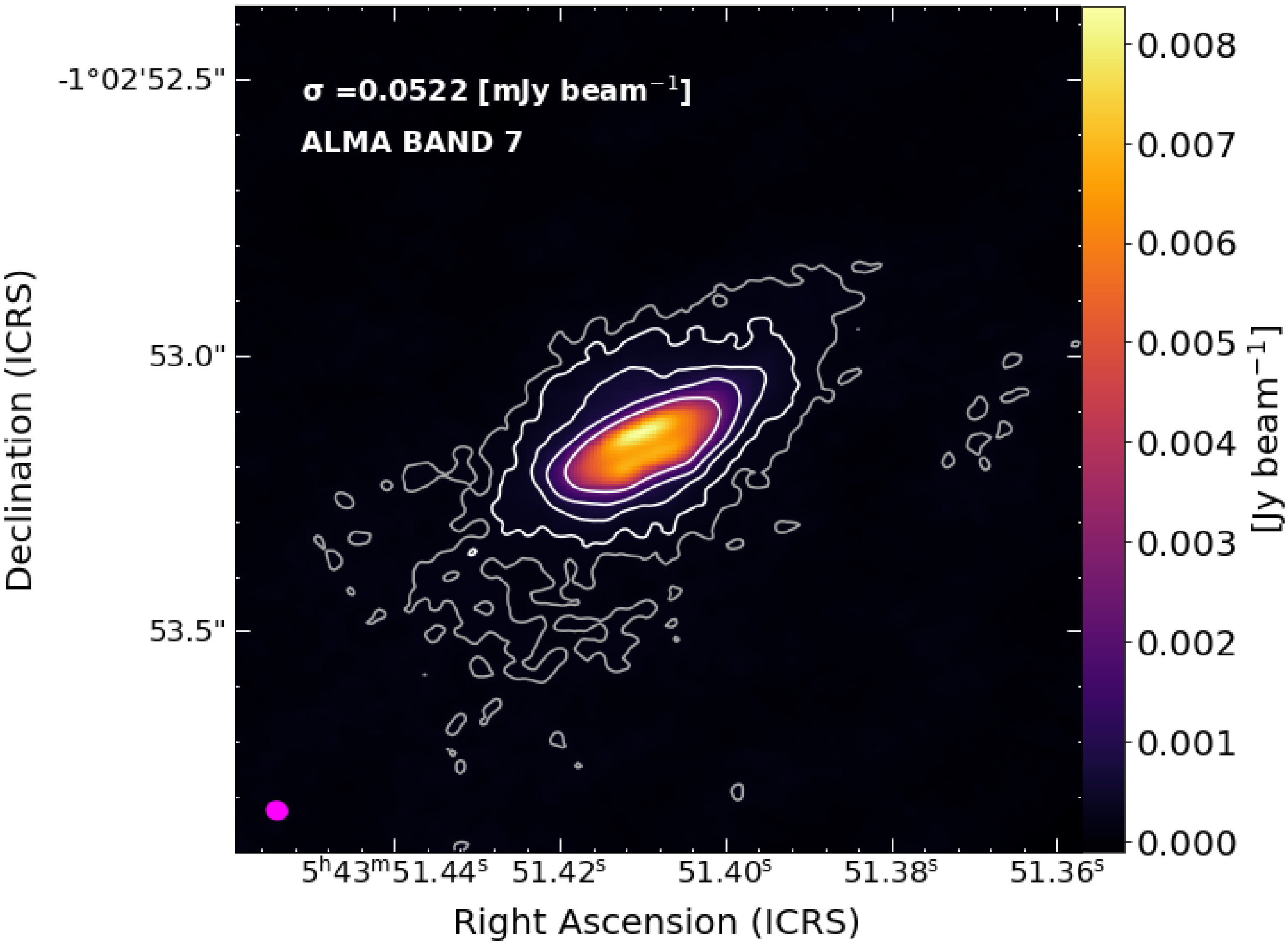

Figure 4: A Band 7 image of HH212 was obtained by combining four previous observations of HH212 (see Table 3). The outermost grey contour line is 3σ and the rest of the contours are 5σ, 10σ, 20σ and 50σ. σ is 0.0522 mJy beam^{-1} as reported on the figure and in Table 1.

3. DISCUSSION

3.1. *HH212 Dust Morphology*

When searching for dust in the wind, it is important to consider where we expect to see this dust and what sizes we expected the grains to be. Dust kinematics is an incredibly complex astrochemical process, but we can make some initial estimates to characterize the grains. First, we expect the dust to be relatively close to the protostar, and we expect these dust grains to be small (on the order of millimeter to sub-micron). We make these estimates based on a brief analysis of the stopping time. The stopping time represents the timescale on which gas from the stellar outflow is expected to have a substantial affect on the trajectory of the dust particle. Different drag forces dominate the stopping time depending on the dust size relative to the mean free path of the gas molecules. (Popovas et al. 2019) For typical nebula the drag force is in the particle regime and is known as Epstein drag. For small spherical grains in the the Epstein drag regime the stopping time is represented by the following equation:

$$t_s = \frac{\rho_{\cdot} s}{\rho v_{\rm th}}, \tag{1}$$

where $\rho_{\cdot}$ is the solid density of dust, $v_{\rm th}$ is the thermal velocity, s is the size of the dust, and ρ is the density of the gas in the nebula. We adopt the $\rho_{\cdot}$ value of 3 g/cm^3 used in Popovas et al. (2019). The dust size range is chosen to be

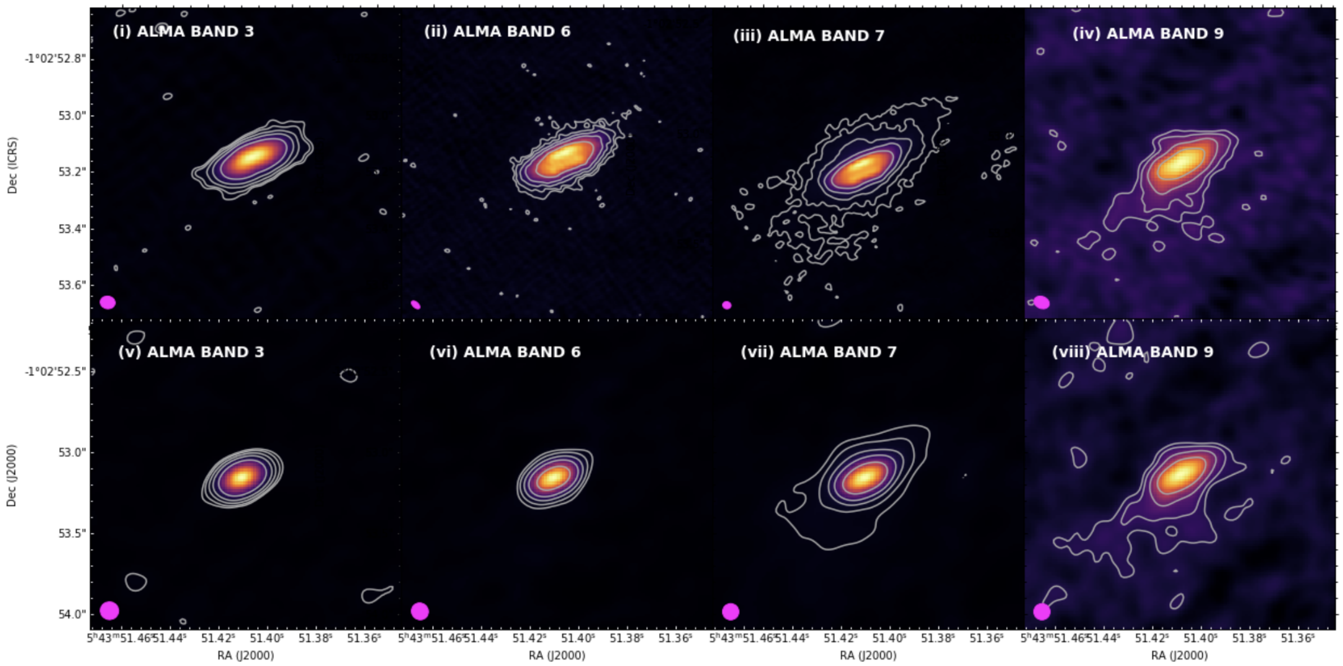

Figure 5: The first row of the figure presents images across ALMA Bands at their natural cell and beam size. The second row presents images across ALMA Bands convolved to the same beam and cell size using the Band 9 image as a template. Contours are drawn at 3σ, 5σ, 10σ, 20σ and 50σ for every image. The color scale is not normalized across each image, but rather the scaling in each panel is according to the peak intensity of each image. More information about image-specific parameters can be found in Table 1.

Table 1: Multi-Band Data and Imaging Parameters

Project ID	**Band**	**Smoothed**	**MarxMin Beam**	**PA**	**Cell Size**	σ	**Total Flux**
			arcsec	°	arcsec	[mJy beam^{-1}]	MJy
2017.1.00712.S	3	No	0.0526 x 0.0444	71.70	0.011	0.000857	1.75
2017.1.00712.S	6	No	0.0359 x 0.0192	48.02	0.005	0.00265	2.94
Combined Band 7*	7	No	0.0375 x 00325	77.31	0.0059	0.0522	1.10
2012.1.00122.S	9	No	0.0804 x 0.0612	66.71	0.016	2.26	2.59
2017.1.00712.S	3	Yes	0.1 x 0.1	0	0.016	0.0192	9.18
2017.1.00712.S	6	Yes	0.1 x 0.1	0	0.016	0.25	4.64
Combined Band 7*	7	Yes	0.1 x 0.1	0	0.016	0.35	1.28
2012.1.00122.S	9	Yes	0.1 x 0.1	0	0.016	3.15	6.57

Observational and image parameters on the data used to create Figure 5. Images that are indicated as 'smoothed' were convolved to the same beam size, using CASA task imsmooth. The images were further regridded to be the same cell size using CASA task imregrid with the smoothed Band 9 used as the template image. *The Band 7 images are not associated with a project code because it is the combination image obtained by combining four project codes.

0.01 micron to 1 mm, to reflect the size of grains that are expected during star formation and young disk phase. The thermal velocity is held constant at 2500 m/s. Finally, the densities are defined as a range from 10 ^{6} to 10^{12} cm^{-3}. This range is constrained by the densities that are seen in protostellar cores and disks. We expect that the stopping time is small for small dust particles and increases proportionally to particle size, and decreases as density increases. The dust in the size range we are looking for is mostly like to be seen with a small stopping time, so we expect to be able to see dust grains of small size, high thermal velocity and low density. Therefore, if there is dust present in the

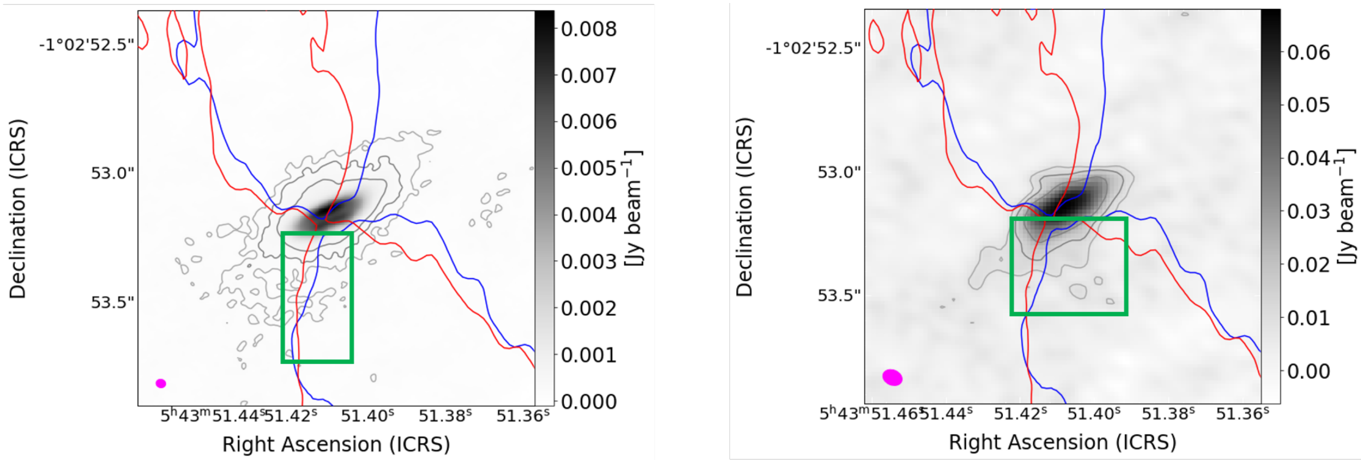

Figure 6: This figure present 12CO(3-2) data from project 2016.1.01475.S overlayed on Band 7 and Band 9 data respectively. More information about image parameters can be found in Table 1. This figure uses data at the natural cell and beam sizes The systemic velocity of the system is 1.6 ± 0.1 km s^{-1}. All channels within 4 km s^{-1} are shown in this figure for the red and blue shifted jets respectively. The green box indicates region of continuum extension coincident with the outflow cavity wall.

outflow of protostellar objects, we expect to see small grains (visible in higher ALMA bands) relatively close to the protostellar core.

An observational confirmation of this phenomenon is suggested by Figure 5. In this figure the continuum observations in ALMA bands 3 and 6 are relatively Gaussian, with regions where there may be only a tentative deviation. However, ALMA bands 7 and 9 show an entirely different picture. The band 7 and 9 images show significant extension of the continuum in the south-west direction both at natural and convolved beam sizes. There is significant loss of detail in the Band 7 convolution due to the size difference of the original beams. 12CO(3-2) is a known outflow tracer, and Figure 6 shows 3σ contour lines for the red and blue shifted outflows overlayed on the Band 7 and Band 9 continuum images. The extension in the continuum appears to be coincident with the outflow cavity wall (see the region within the green box), suggesting that some of the extension may be dust carried away by the disk wind. Some of the extension does not overlap with the outflow cavity wall, further suggesting that some of the detected extension may in fact be infall or another phenomena. However, we believe that it is unlikely that the dust coincident with the outflow cavity wall can be related to infall, as the outflow is pushing gas away from the circumstellar disks in that region. 12CO(2-1) is another commonly used outflow tracer, but at this time no observations of 12CO(2-1) for HH212 at sufficient angular resolution exist in the ASA. ALMA is capable of observing a multitude of molecular lines, and other molecular lines were observed simultaneously for some of the same projects that we present here. The ASA has molecular line data at sufficient resolution (associated with the projects in Table 1) for other known outflow, disk and shock tracers. Further constraints can be made about the extension by inspecting other known outflow tracers, as well as lines from other parts of the protostellar system.

3.2. *Spectral Index Map*

In order to determine if it is possible for dust to be lifted by the wind we need to constrain the size distribution of the dust grains. The spectral index, commonly denoted as α, is the dependence of radiative flux per unit frequency, or wavelength. The spectral index α (given by Equation 2) is defined as:

$$\alpha = \frac{ln(S_{\nu 1}/S_{\nu 2})}{ln(\nu_1/\nu_2)} \tag{2}$$

and is shown in Figure 7 where alpha is plotted between Band 7 and Band 9. The spectral index is notably different in the disk region compared to the region of extension. The higher value of spectral index in the extension

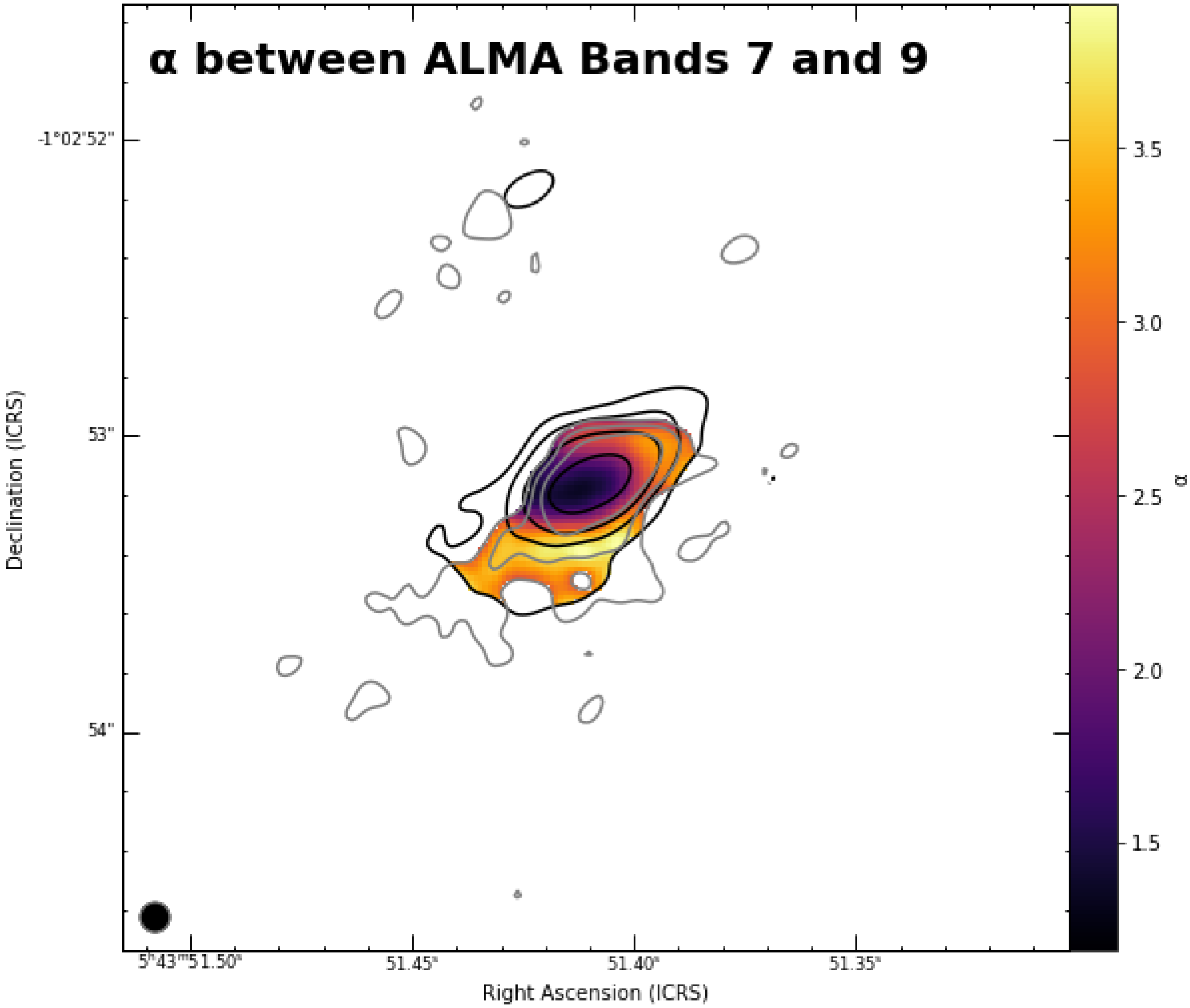

Figure 7: Spectral Index α between ALMA Band 7 and Band 9. Both observations have been smoothed to 0.1" beam size and 0.016" cell size. The contours are drawn at 3σ,5σ, 10σ, 20σ and 50σ with black contours corresponding to the Band 7 data and grey corresponding to Band 9. 3σ of Band 7 is 0.00105 Jy and 3σ of Band 9 is 0.00945 Jy.

suggests that there is stronger emission from the Band 9 data in that region, indicating the presence of smaller dust grains.

3.3. *Dust Mass Estimation from Observational Emission*

In order to determine how the initial conditions for planetary formation may be affected by lifting dust from the disk, we calculate how much mass is calculated from the emission in both the entire disk region, and the region of extended continuum.

$$M_\lambda = \frac{Scd^2}{B_\lambda(T)\kappa\lambda^2} \tag{3}$$

In Equation 3, S is the flux [mJy], d is the distance to the star [pc], κ is the opacity as determined by the grain size of the dust [cm^2/g^{-1}], and $B_\lambda(T)$is the wavelength Plank function [J/[ms^{-1}]] as follows:

$$B_\lambda(T) = \frac{2hc^2}{\lambda^5 e^{hc/\lambda k_B T} - 1} \tag{4}$$

Equation 3 is adapted from Equation 1 of Motte & André (2001) using the relationship between the frequency based Planck function and the wavelength-based Planck function (different only by a factor of c/λ^2). Equation 4 is the wavelength-dependent Planck function. Calculations were made assuming 100K and an opacity of $0.014[cm^2/g^{-1}]$, following Bjerkeli et al. (2019), although we have chosen a slightly lower temperature since we are not looking at the outflow exclusively.

The amount of mass was calculated based on emission in the entire disk (Bands 3, 6, 7, 9) and in the region of extended continuum (Bands 7, 9) using Equation 3. More details on the results of the mass calculation can be found in Table 2. The calculated mass in the Band 7 extension is 5 to 7% of the total disk mask, depending on the exact region that was defined. The different regions are detailed in Table 2, with the 3 - 5σ region being well separated from the disk and 5 - 10σ region being close to the interface of the disk. The calculated mass in the Band 9 extension is 14 to 21.5% of the total disk mask. These percentages are a non-trivial amount of mass, suggesting that a significant amount of small dust grains are in the extended regions. The mass calculation is highly dependant on the region that is defined as the "extension", here it is defined as the region within the green boxes defined in Figure 6. The Mass of dust emission is also highly dependent on the temperature and changing the temperature by a factor of 2 changed the mass by a factor of 0.5 - 2 dependant on the region. However, regardless of the temperature the total percentage of the dust mass in the extension is a significant percent of the total calculated disk mass.

Table 2: Mass Estimates in Disk and Extension Across All Bands

Region	**Sigma Range**	**Flux Estimate**	**Estimated Mass**	**Percent of Total Mass**
	σ	[mJy beam^{-1}]	Solar Masses	
Band 7 Entire Disk	3 to 100	7.3	0.013	100
Band 7 Entire Disk	3 to 5	0.83	0.0014	10.6
Band 7 Entire Disk	5 to 10	0.66	0.0012	9.09
Band 7 Extension	3 to 100	0.61	0.0011	8.4
Band 7 Extension	3 to 5	0.36	0.0006	4.9
Band 7 Extension	5 to 10	0.15	0.0002	2.1
Band 9 Entire Disk	3 to 100	17.5	0.0116	100
Band 9 Entire Disk	3 to 5	3.9	0.0027	23.1
Band 9 Entire Disk	5 to 10	3.2	0.0021	18.5
Band 9 Extension	3 to 100	4.3	0.0028	24.3
Band 9 Extension	3 to 5	2.4	0.0016	13.8
Band 9 Extension	5 to 10	1.4	0.0009	7.9
Band 6 Entire Disk	3 to 100	1.17	0.010	100
Band 3 Entire Disk	3 to 100	1.9	0.0240	100

This table shows the amount of mass from emission for each of the defined regions using Equation 3. The values of 3σ in mJy beam^{-1} for the band 3 calculation is 0.02, the band 6 is 0.07, the band 7 is 0.15 and the band 9 is 6.79. Percentage of the total mass is determined assuming that the mass in the 3-100 region for each respective band is 100 percent of the mass that is calculated from the emission. Calculations were made assuming 100K and an opacity of 0.014 cm^2/g.

4. CONCLUSIONS

Here we present the case of HH212 as the source with the first observational detection of sub-millimeter dust being lifted from the accretion disk by the outflow. The spectral index indicates that there are small dust grains in the region coincident with the outflow cavity wall and our mass calculations indicate that this amount of dust is non-trivial, compared to the mass of the disk. Furthermore the detection of this dust gives support to the theory of disk wind as the launching mechanism of molecular outflows in young protostellar systems.

The entirety of the extension is not perfectly aligned with the outflow which suggests that in addition to dust in the outflow, some of the dust may be infalling from the outer envelope to the disk.

Further observations are needed to confirm the observational detection of dust near the outflow cavity wall of HH212. We would like to obtain high resolution observations of Bands 5 and 8, and observations in Band 6 at sufficient resolution to investigate if the extension is coincident with 12CO(2-1) data. We have submitted a proposal for ALMA cycle 8 requesting the observations necessary to confirm the detection.

ACKNOWLEDGMENTS

The author would like to thank Adele Plunkett (NRAO), Jonathan Ramsey (UVA) and Per Bjerkeli (Chalmers) for their guidance and advice on this project. The National Radio Astronomy Observatory (NRAO) is a facility of the National Science Foundation operated under cooperative agreement by Associated Universities, Inc. This project was completed as part of a student internship program at NRAO. The authors would like to thank the student group at the Chalmers University of Technology: Johanna Matero, Madeleine Karlsson, Viktor Martvall, Ajša Ćuprija and Veronica Jannisa, as well as Daniel Lin at the University of Virginia, for their work in identifying protostellar sources for this project. The authors would also like to thank the NRAO data analysts and the Virginia Initiative in Cosmic Origins without whom this project would have been impossible. The authors acknowledge support from the NASA Astrophysics Theory Program under grant no. 80NSSC20K0533.

APPENDIX

Table 3: Data and Imaging Parameters for Band 7 Combination

Project ID	**Maj x Min Beam**	**PA**	**Cell Size**	**Peak Flux**	**Total Flux**	σ
	arcsec	degrees	units	[Jy beam^{-1}]	[Jy beam^{-1}]	[Jy beam^{-1}]
2012.1.00122.S	0.1996 x 0.1346	85.46	0.075	0.010	0.200	0.002
2015.1.00024.S	0.0205 x 0.0185	-71.25	0.0034	0.003	0.112	0.00016
2016.1.01475.S(x259)	0.0963 x 0.0922	-46.67	0.019	0.003	0.013	0.0022
2016.1.01475.S(x25b)	0.3912 x 0.2825	-69.54	0.0036	0.135	0.210	0.0036
2017.1.00044.S	0.0365 x 0.0331	-81.62	0.0065	0.033	0.140	0.00064

Observational parameters of each project that was combined to form the 345 GHz continuum image in Figure 4.

REFERENCES

Bjerkeli, P., Ramsey, J. P., Harsono, D., et al. 2019, A&A, 631, A64, doi: 10.1051/0004-6361/201935948

Bouvier, J., Matt, S. P., Mohanty, S., et al. 2014, in Protostars and Planets VI, ed. H. Beuther, R. S. Klessen, C. P. Dullemond, & T. Henning, 433, doi: 10.2458/azu_uapress_9780816531240-ch019

Claussen, M. J., Marvel, K. B., Wootten, A., & Wilking, B. A. 1998, ApJL, 507, L79, doi: 10.1086/311669

Frank, A., Ray, T. P., Cabrit, S., et al. 2014, in Protostars and Planets VI, ed. H. Beuther, R. S. Klessen, C. P. Dullemond, & T. Henning, 451, doi: 10.2458/azu_uapress_9780816531240-ch020

Kounkel, M., Covey, K., Suárez, G., et al. 2018, AJ, 156, 84, doi: 10.3847/1538-3881/aad1f1

Lee, C.-F., Li, Z.-Y., Ho, P. T. P., et al. 2017, Science Advances, 3, e1602935, doi: 10.1126/sciadv.1602935

Lee, C.-F., Li, Z.-Y., Codella, C., et al. 2018, The Astrophysical Journal, 856, doi: 10.3847/1538-4357/aaae6d

Motte, F., & André, P. 2001, A&A, 365, 440, doi: 10.1051/0004-6361:20000072

Persson, M. V. 2014, Current view of protostellar evolution (ENG), figshare, doi: 10.6084/m9.figshare.654555.v7

Popovas, A., Nordlund, A., & Ramsey, J. 2019, Monthly Notices of the Royal Astronomical Society: Letters, 482, L107, doi: 10.1093/mnrasl/sly197

Scott, E. R. D., Krot, A. N., & Sanders, I. S. 2018, ApJ, 854, 164, doi: 10.3847/1538-4357/aaa5a5

Shang, H., Allen, A., Li, Z.-Y., et al. 2006, ApJ, 649, 845, doi: 10.1086/506513

Tabone, B., Cabrit, S., Pineau des Forêts, G., et al. 2020, A&A, 640, A82, doi: 10.1051/0004-6361/201834377

Testi, L., Birnstiel, T., Ricci, L., et al. 2014, in Protostars and Planets VI, ed. H. Beuther, R. S. Klessen, C. P. Dullemond, & T. Henning, 339, doi: 10.2458/azu_uapress_9780816531240-ch015

Yen, H.-W., Zhao, B., Koch, P., et al. 2020, The Astrophysical Journal, 893, 54, doi: 10.3847/1538-4357/ab7eb3